⌘ *Author's Choice*

THE JOURNAL OF BIOLOGICAL CHEMISTRY VOL. 286, NO. 26, pp. 23570–23581, July 1, 2011

Transport Mechanism and pH Regulation of the Na^+/H^+ Antiporter NhaA from *Escherichia coli*

AN ELECTROPHYSIOLOGICAL STUDY[*] [S]

Received for publication, February 15, 2011, and in revised form, April 8, 2011 Published, JBC Papers in Press, May 12, 2011, DOI 10.1074/jbc.M111.230235

Thomas Mager[‡], Abraham Rimon[§], Etana Padan[§1], and Klaus Fendler[‡2]

From the [‡]Max-Planck-Institut für Biophysik, 60438 Frankfurt/Main, Germany and the [§]Institute of Life Sciences, Hebrew University of Jerusalem, 91904 Jerusalem, Israel

Using an electrophysiological assay the activity of NhaA was tested in a wide pH range from pH 5.0 to 9.5. Forward and reverse transport directions were investigated at zero membrane potential using preparations with inside-out and right side-out-oriented transporters with Na^+ or H^+ gradients as the driving force. Under symmetrical pH conditions with a Na^+ gradient for activation, both the wt and the pH-shifted G338S variant exhibit highly symmetrical transport activity with bell-shaped pH dependences, but the optimal pH was shifted 1.8 pH units to the acidic range in the variant. In both strains the pH dependence was associated with a systematic increase of the K_m for Na^+ at acidic pH. Under symmetrical Na^+ concentration with a pH gradient for NhaA activation, an unexpected novel characteristic of the antiporter was revealed; rather than being down-regulated, it remained active even at pH as low as 5. These data allowed a transport mechanism to advance based on competing Na^+ and H^+ binding to a common transport site and a kinetic model to develop quantitatively explaining the experimental results. In support of these results, both alkaline pH and Na^+ induced the conformational change of NhaA associated with NhaA cation translocation as demonstrated here by trypsin digestion. Furthermore, Na^+ translocation was found to be associated with the displacement of a negative charge. In conclusion, the electrophysiological assay allows the revelation of the mechanism of NhaA antiport and sheds new light on the concept of NhaA pH regulation.

The Na^+/H^+ exchanger NhaA is essential for the Na^+ and H^+ homeostasis in *Escherichia coli* (1), and its homologues are widely spread in enterobacteria and found even in human (2). NhaA transports two H^+ ions in exchange for one Na^+ ion across the bacterial membrane. Compared with other transporters, its transport capacity is extremely high. Turnover numbers of up to 1000 s^{-1} have been reported (3).

Drastic pH dependence is characteristic of many eukaryotic and prokaryotic Na^+/H^+ antiporters (for review, see Ref. 4). NhaA has been shown to be active at pH 8.5 and inactive at pH 6.5 (3). The pH dependence of the transporter activity is paralleled with conformational changes of the enzyme, which could be monitored with various techniques like tryptic digestion (5, 6), monoclonal antibody binding (7), fluorescence resonance energy transfer (8), accessibility testing of Cys replacement mutations to various SH reagents (9, 10), cryoelectron microscopy (11), and Fourier transform infrared spectroscopy (12). It is believed that this pH-dependent conformational transition(s) converts the transporter into an "inactive" state at acidic pH (13). Various mutants have been investigated (14, 15) that show an altered pH dependence. A prominent member of this family is G338S NhaA. This transporter shows a distinct pH shift of inactivation and was initially described as a "pH independent" transporter (16).

In general, secondary active transporters are believed to function according to an alternative access model (17); transport is brought about by providing alternative access of a common binding site to both sides of the membrane. This could be a rocker switch-like domain movement in the protein as proposed for the sugar/H^+ cotransporter LacY (18) or a more subtle one-helix bending or displacement as proposed for NhaA (see *e.g.* Refs. 11, 19 and 20). In any case, conformational transitions are most probably involved in substrate transport of NhaA, although their exact nature has yet to be determined.

The conformational transitions believed to be involved in NhaA pH regulation are distinct from the transport related ones. For example, it was suggested that at acidic pH an inactive acid-locked state exists where the periplasmic passage is blocked by an ion barrier (19, 21, 22). With increasing pH a signal from a putative "pH sensor" would remove the barrier and restore NhaA activity. A similar mechanism of pH regulation involves a disordered N terminus, and its pH-dependent ordering would restore activity at alkaline pH (11). These mechanisms have in common that they act in an allosteric manner and differ from the intrinsic pH dependence of the active site caused by the substrate proton.

The above described mechanisms of substrate transport and pH regulation have been derived from extensive biochemical, biophysical computational and structural studies. Here we have undertaken another approach, solid supported membrane

* This work was supported by the Deutsche Forschungsgemeinschaft SFB 807.

[S] The on-line version of this article (available at http://www.jbc.org) contains supplemental Figs. 1–3.

⌘ *Author's Choice*—Final version full access.

[1] Supported by EDICT (European Drug Initiative on Channels and Transporters) Grant EU EP7 and by USA-Israel Binational Science Foundation Grant BSF#20050130.

[2] To whom correspondence should be addressed: Max-Planck-Institut für Biophysik, Max-von-Laue Str. 3, 60438 Frankfurt/Main, Germany. Fax: 49-69-63032204; E-mail: fendler@biophys.mpg.de.

(SSM)[3]-based electrophysiology (23), which allows measurement of the NhaA activity under well defined conditions on both sides of the membrane. The aim of the study was to test whether and to what extent the pH dependence of NhaA is determined by allosteric pH regulation and/or by the intrinsic dependence of transport on the concentration of the substrate protons. Related to this issue is the question of whether the observed conformational transitions are regulative or part of the transport mechanism.

EXPERIMENTAL PROCEDURES

Overexpression and Purification of wt- and G338S-NhaA—C-terminal-His-tagged wt- and G338S-NhaA were overexpressed and purified on a Ni^{2+}-NTA column as previously described (24). Purified proteins in 25 mM potassium acetate (pH 5), 100 mM KCl, 5 mM $MgCl_2$, 0.03% DDM were stored at 4 °C until reconstitution.

Reconstitution of Proteoliposomes—Reconstitution of purified wild type or G338S mutant was carried out with *Escherichia coli* phospholipids (Avanti Polar Lipids). The lipid was evaporated under constant nitrogen flow and rotation. Then a buffer containing 25 mM Hepes, 25 mM Tris-HCl, 100 mM KCl, and 2 mM DTT (pH 7) was added to a final concentration of 10 mg/ml. The lipid suspension was extruded through a 400-nm filter. After extrusion, the liposomes had a mean diameter of 200–300 nm, measured by dynamic light scattering (Zeta Plus, Brookhaven Instrument Corp.). Subsequently, 1% (w/v) β-D-octylglucoside and purified wt- or G338S-NhaA in mass ratios of 1:10–1:50 to the lipid content were added. Removal of detergent was accomplished by adding 30% (v/v) polystyrene beads (Bio-Beads, Bio-Rad) followed by constant shaking at 4 °C overnight. After the polystyrene beads were exchanged for fresh ones, shaking was continued for 1 additional hour at 4 °C. After removal of the polystyrene beads, the proteoliposomes were centrifuged (130,000 × *g*, 4 °C, 1 h) and resuspended in 300 mM KCl, 75 mM MOPS, 5 mM $MgCl_2$, and 1 mM DTT (pH 7) to a lipid concentration of 5 mg/ml. The proteoliposomes were frozen in liquid nitrogen and stored at −80 °C until use. Prior to the SSM measurements, the samples were gently sonicated with cooling breaks on ice until the suspensions became translucent.

Production of wt- and G338S-NhaA Inside-out Vesicles—Production of inside out (ISO) membrane vesicles was performed by disruption of wt- or G338S-NhaA overexpressing *E. coli* with a French press (20,000 p.s.i.). Bacterial debris were removed by centrifugation at 10,000 × *g* for 10 min. The ISO membrane vesicles were further purified by metal affinity two-phase partitioning according to Everberg *et al.* (25). Purification of ISO vesicles via a two-phase system in combination with Ni^{2+}-NTA agarose resin was possible, as the His tag is cytoplasmatically located and, therefore, exposed in ISO vesicles.

SSM-based Electrophysiology—SSM measurements were performed as described previously (23). Briefly 45 μl of proteoliposomes at a lipid concentration of 5 mg/ml or ISO membrane vesicles at a total membrane protein concentration of 1.5 mg/ml were adsorbed to an octadecanethiol/phospholipid hybrid bilayer on a gold surface (sensor). Proteoliposomes were allowed to adsorb to the sensor for 2–3 h. Adsorption of the ISO membrane vesicles was carried out for 3–12 h. By means of solution exchange protocols, electrogenic transport was initiated by a rapid change of substrate ion concentration. SSM measurements were performed according to a single solution exchange protocol (nonactivating solution, 0.5 s; activating solution, 0.5 s; nonactivating solution, 0.5 s) or a double solution exchange protocol (resting solution, 0.75 s; nonactivating solution, 0.8 s; activating solution, 0.5 s; nonactivating solution, 0.5 s; resting solution, 1 s). The double solution exchange protocol allowed separation of the pH artifact from the transporter-derived transient. Currents, recorded throughout the measurements, were amplified with a current amplifier set to a gain of 10^8-10^{10} V/A and low pass filtering set to 2000 Hz. To minimize Na^+ concentration jump artifacts, sodium was replaced by an equal amount on an inert cation (K^+ or choline) in the nonactivating solution. In addition, the ionic strength was kept high by adding choline$^+$ or K^+ to a total cation concentration of 305 mM. Details concerning the composition of the solutions are given in the figure legends.

Data Analysis—The current generated by the transporter is distorted by capacitive coupling via the network of the compound membrane formed by the SSM and the adsorbed liposomes (23). In particular a characteristic time constant of the network τ is introduced into the signal, which was determined by an appropriate mono-exponential least-squares fit. Neglecting a constant scaling factor, the transporter current I_{rec} can be reconstructed from the measured current $I(t)$ using,

$$I_{rec}(t) = I(t) + \frac{1}{\tau}\int_0^t I(t)dt \qquad \text{(Eq. 1)}$$

For details see the supplemental Figs. 1–2.

In general, three different data sets from three individual sensors were recorded for a substrate dependence. The peak currents of each Na^+ dependence and Na^+ gradient as well as pH gradient driven were normalized to the corresponding V_{max} values resulting from a hyperbolic fit to the individual data sets and then averaged. Although data for a specific figure were obtained with a single proteoliposome or membrane preparation, various preparations were tested throughout this study, yielding essentially the same results.

To describe the pH dependence of the transport activity after a Na^+ concentration jump, peak currents I_{peak} as well as the stationary component of reconstructed pump currents I_{rec} were displayed. The currents (I_{peak} or I_{rec}) of each individual pH dependence at 10 and 100 mM Na^+ (3–4 data sets) were first normalized to the scaling parameter A of the minimal-model turnover fit and then averaged. For presentation, the averaged currents were finally normalized to their maximal value at 100 mM Na^+. For a detailed description of the minimal model, see the supplemental Fig. 3.

Na^+ Dependence of wt-NhaA Trypsin Digestion—Purified NhaA (5 μg) was resuspended in a 0.5-ml reaction mixture

[3] The abbreviations used are: SSM, solid supported membrane; ISO, inside out; RSO, right side out.

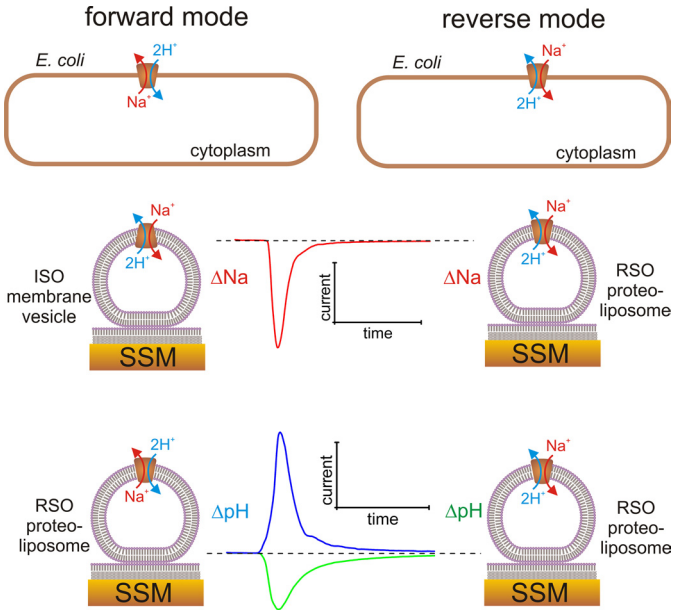

FIGURE 1. **Transport modes of NhaA in the bacterial cell and under experimental conditions.** The *left column* shows the forward transport mode of NhaA corresponding to its physiological transport direction in *E. coli*, and the *right column* shows the reverse transport mode. In the *upper panel* a graphic representation of both transport modes in the bacterial cell is given. The *lower two panels* show the experimental preparations used for the investigation of the two transport modes. Na^+ gradient (ΔNa)- or pH gradient (ΔpH)-driven transport activity of NhaA and the corresponding transient currents observed on the SSM are schematically depicted. Note the different polarity of the currents at different conditions.

containing 0.1 M choline chloride, 0.7 mM EDTA/K^+, 1 mM $CaCl_2$, 0.1% dodecyl maltoside, 50 mM HEPES/Tris at the indicated pH values with or without the indicated concentration of NaCl. At zero time, 0.1 μg of trypsin (Sigma, type III from bovine pancreas) was added, the reaction mixture was incubated at 37 °C for 1 h, and the reaction was terminated by the addition of trypsin inhibitor (Sigma, type II). The protein was precipitated in 10% trichloroacetic acid for 30 min at 4 °C, centrifuged (21,000 × *g* for 30 min 4 °C), resuspended in sampling buffer, separated on SDS-PAGE, and Coomassie Blue-stained, and the band density was quantified by Image Gauge (Fuji) software.

RESULTS

Membrane vesicles prepared from bacteria overexpressing wild type (wt) or G338S NhaA and liposomes reconstituted with purified wt or G338S NhaA were analyzed using SSM-based electrophysiology. Membrane vesicles prepared by French press cell disruption have an ISO orientation (27). We have further ensured complete ISO orientation of the vesicles by using an extraction procedure with nickel-nitrilotriacetic acid-tagged beads (see "Experimental Procedures"). As shown previously, in the proteoliposomes, NhaA is in a right-side out (RSO) orientation (28). The two preparations enabled us to investigate the kinetics of the transporter in the forward and reverse modes (Fig. 1). Here the terms "forward" and "reverse" mode refer to the physiological transport direction of NhaA, where Na^+ is transported from the cytoplasmic to the periplasmic side of the protein, whereas H^+ moves in the opposite direction or vice versa, respectively. Na^+ gradient (ΔNa)-driven transport was investigated on the SSM by applying an inward-directed Na^+ gradient (Na^+ inside = 0) to the membrane vesicles or proteoliposomes. Therefore, ΔNa-driven transport corresponds to the forward mode in ISO membrane vesicles and to the reverse mode in RSO proteoliposomes. H^+ gradient (ΔpH)-driven transport was studied only with RSO proteoliposomes using inside and outside-directed gradients, which again allowed the investigation of the forward and reverse transport modes.

Membrane vesicles or proteoliposomes were adsorbed to the SSM, and transport was initiated by applying a pH or a Na^+ concentration jump (Fig. 1). This generated a transient current in the capacitively coupled system (23). In general, the observed transient currents represent the stationary transport activity of NhaA (28), and the peak currents were taken to quantify the activity (23). Only under extreme conditions were presteady-state current components observed in the signal (see Fig. 6). To account for this, the NhaA transporter current was numerically reconstructed using the properties of the capacitively coupled system (see "Experimental Procedures"), and the stationary component of the reconstructed transporter current was determined. In comparison it was found that reconstructed currents and peak currents yield essentially the same results (see Fig. 2). In the following we will use only the peak currents and consider them as a reliable measure of the transporter steady-state activity.

pH Dependence of wt and G338S NhaA—To compare the transport properties of G338S NhaA and wt NhaA, the pH dependence of ΔNa-driven transport was investigated using SSM measurements. Therefore, concentration jumps of 10 and 100 mM Na^+ were performed at pH values of pH 5 to 8 for G338S NhaA and at pH values of pH 6 to 9.5 for wt NhaA (Fig. 2). The pH dependence of transport was investigated in forward (Fig. 2, *A*, *C*, and *E*) and reverse transport direction (Fig. 2, *B*, *D*, and *F*) using ISO membrane vesicles and RSO proteoliposomes, respectively. Transient currents are shown in Fig. 2, *A* and *B*. In agreement with the $1Na^+/2H^+$ stoichiometry of NhaA, ΔNa-driven transport results in a negative current (Fig. 2, *A* and *B*). Because the transporter currents of the ISO preparation are small, positive solution exchange artifacts superimpose the signal, resulting in biphasic current transients (Fig. 2*A*). The peak currents (Fig. 2, *C* and *D*) as well as the stationary component of reconstructed transporter currents (Fig. 2, *E* and *F*) are displayed. As is apparent in the figure, peak currents and reconstructed stationary currents are hardly different.

wt NhaA, after a 100 mM Na^+ jump at pH 8.5, yielded peak currents of −1.2 ± 0.3 nA for ISO membrane vesicles and −12 ± 2 nA for RSO proteoliposomes. G338S NhaA peak currents after a 100 mM Na^+ jump at pH 7 were −1.6 ± 0.7 nA for RSO proteoliposomes and −1.2 ± 0.4 nA for ISO membrane vesicles. At pH 6, after a 100 mM Na^+ jump, wt NhaA transient currents were of positive polarity with peak currents of 129 ± 63 pA for RSO proteoliposomes and 213 ± 120 pA for ISO membrane vesicles. The same was observed at pH 5 after a 100 mM Na^+ jump using G338S NhaA with peak currents of 180 ± 20 pA for RSO proteoliposomes and 140 ± 40 pA for ISO membrane vesicles. The positive transient currents closely resem-

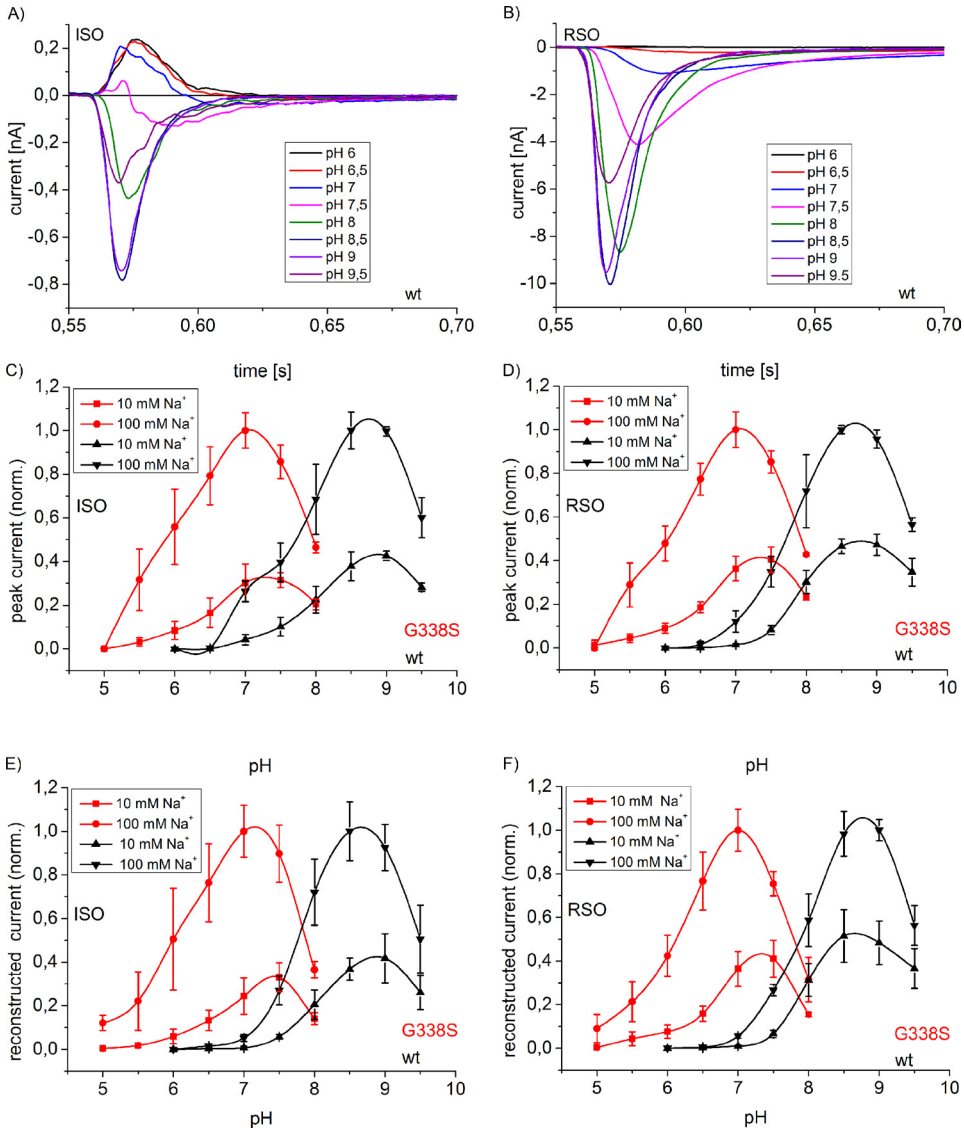

FIGURE 2. **pH dependence of transient currents obtained with wt- and G338S-NhaA after a Na^+ concentration jump using the single solution exchange protocol.** *A* and *B*, typical transient currents were recorded after a 100 mM Na^+ concentration jump using RSO proteoliposomes and ISO membrane vesicles. Signals of ISO membrane vesicles are a superposition of the NhaA transporter current (negative phase) and the solution exchange artifact (positive phase). Signals of RSO proteoliposomes are so large that the contribution of artifacts is negligible. *C* and *D*, normalized peak currents at the indicated pH values were subtracted by the Na^+ jump artifact. *E* and *F*, shown are normalized reconstructed stationary currents at the indicated pH values. The graphs show average values from recordings using three individual sensors and the corresponding S.D. Currents are normalized as described under "Experimental Procedures." *A*, *C*, and *E*, ISO membrane vesicles with G338S NhaA (*red*) or wt NhaA (*black*) are shown. *B*, *D*, and *F*, RSO proteoliposomes (LPR = 10) with G338S NhaA (*red*) or wt NhaA (*black*) are shown. For the Na^+ concentration jumps, activating solutions containing 10 mM NaCl and 290 mM KCl or 100 mM NaCl and 200 mM KCl titrated to the indicated pH values with HCl or Tris were used. The nonactivating solutions contained 300 mM KCl instead. In addition all buffers contained 5 mM $MgCl_2$, 25 mM Tris, 25 mM MOPS, 25 mM MES, and 1 mM DTT.

bled the Na^+ solution exchange artifact on empty sensors that are caused by ion binding/release to/from the SSM (29). In particular, time constants and peak values for a particular sensor were equal. Therefore, these currents were assigned to Na^+ solution exchange artifacts, and their amplitudes (peak currents) were subtracted from the signal amplitudes.

Comparison of the ΔNa-driven transport in forward (Fig. 2, *C* and *E*) and reverse direction (Fig. 2, *D* and *F*) showed that transport of wt NhaA and G338S NhaA is virtually transport direction-independent at all pH values. G338S NhaA showed a maximal transport activity between pH 7 and 7.5. In contrast, the pH dependence of wt NhaA showed a maximal transport activity between pH 8.5 and 9. At pH values higher and lower than optimal, the currents decreased with the same characteristics for wt NhaA and G338S NhaA. Note that the decrease of the transients at non-optimal pH values was fully reversible throughout the entire pH range shown in the figure. Hence, G338S NhaA is not independent of pH in the physiological pH range. It rather shows a pH dependence shifted by ~1.8 pH units to more acidic pH values compared with the wt.

Na^+ Dependence of the Transport Activity of wt NhaA and G338S NhaA at Intermediate and Low pH—The Na^+ dependence of ΔNa-driven transport of wt NhaA in the forward direction was investigated at pH 8.5, where the transport activity is maximal, and at pH 7.5, where a reduced trans-

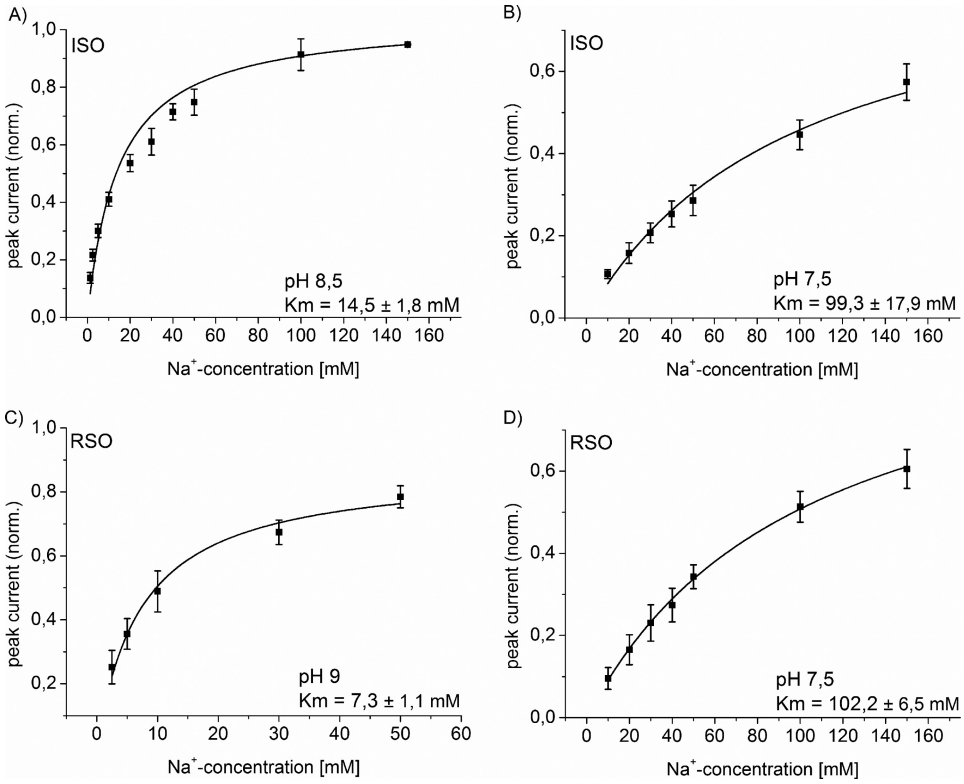

FIGURE 3. **Na^+ concentration dependence of wt NhaA at optimal and acidic pH.** The transient currents were recorded after a Na^+ concentration jump using the single solution exchange protocol. *A* and *B*, normalized peak currents with ISO membrane vesicles are shown. *C* and *D*, normalized peak currents with RSO proteoliposomes (LPR = 10) are shown. The graphs show average values from recordings using three individual sensors and the corresponding S.D. Normalization was as described under "Experimental Procedures." For the Na^+ concentration jumps, activating solutions containing *x* mM NaCl and (300–*x*) mM KCl titrated to the indicated pH values with Tris were used. The nonactivating solutions contained 300 mM KCl instead. In addition, all buffers contained 5 mM $MgCl_2$, 25 mM Tris, 25 mM MOPS, 25 mM MES, and 1 mM DTT. The *solid line* is a fit to the data using a hyperbolic model function with a half-saturation concentration K_m and a fixed $v_{max} = 1$.

TABLE 1

ΔNa-driven transport using ISO and RSO preparations

Kinetic parameters for wt and G338S NhaA were determined from the Na^+ dependencies (K_m^{Na}, Figs. 3 and 4) and the pH dependencies (K_D^{Na}, pK, and k_2/k_1; Fig. 9) using the minimal kinetic model in Fig. 8. *, value was taken from Zuber et al (28).

Wt					
	K_m^{Na}(pH 8.5)	K_m^{Na} (pH 7.5)	K_D^{Na}	pK	k_2/k_1
ISO forward	14.5 ± 1.8	99 ± 18	4.1 ± 1.5	8.7 ± 0.1	7
RSO reverse	11 ± 9.7*	102 ± 7	2.6 ± 1.4	8.8 ± 0.2	7
G338S					
	K_m^{Na} (pH 7.0)	K_m^{Na} (pH 6.0)	K_D^{Na}	pK	k_2/k_1
ISO forward	34.6 ± 1.8	153 ± 9	10 ± 4	7.0 ± 0.2	4.6
RSO reverse	30.3 ± 2.2	104 ± 3	12 ± 4	7.0 ± 0.2	3.1

port activity is observed (Fig. 3, *A* and *B*). In the reverse transport direction, the Na^+ dependence was measured at pH 9 and 7.5 (Fig. 3, *C* and *D*). For a direct comparison, data for RSO proteoliposomes at pH 8.5, determined previously (28), are included in Table 1.

The individual data sets obtained with different sensors were fitted with a hyperbolic model function with a half-saturation concentration K_m and a saturation value of v_{max}. A direct comparison of v_{max} at pH 7.5 and 8.5 (ISO) or pH 7.5 and 9.0 was possible, because data for both pH values were determined with the same sensor. The comparison showed that v_{max} did not change significantly when the pH was reduced. In forward transport direction, v_{max} decreased by 30% on average when going from pH 8.5 to 7.5. In reverse transport direction, v_{max} decreased by 20% on average when going from pH 9 to 7.5.

For a comparison of K_m^{Na}, averaged data of different sensors as shown in Fig. 3 were used. In contrast to v_{max}, K_m^{Na} varied significantly with pH (Table 1). As observed for the pH dependence (Fig. 2), the kinetic properties of NhaA in forward and reverse transport direction were similar.

For comparison, the Na^+ dependence of ΔNa-driven transport of G338S NhaA in forward and reverse directions was investigated at pH 7.0 and 6.0 (Fig. 4). A similar analysis as described above for wt NhaA led to the conclusion that also in this case v_{max} did not change significantly with pH, but K_m^{Na} does. Again the kinetic properties of NhaA in forward and reverse transport direction were similar (Table 1).

To estimate a putative influence of Na^+ contaminations introduced into the nominally Na^+-free buffers by the KCl salt, the concentration of Na^+ in the normally used nonactivating solution was determined by atomic absorption spectroscopy to be 100 ± 40 μM. In addition, the concentration dependence was measured with choline chloride instead of KCl and with ultraclean KCl beads. In the latter case, the Na^+ contamination was only 3 μM. With choline chloride and ultraclean KCl beads we obtained a K_m^{Na} = 7.8 ± 0.7 and 6 ± 1 mM, respectively. This is not significantly different from the previously determined value of K_m^{Na} = 11 ± 0.7 mM (28). Therefore, an influence of contaminating Na^+ on the determined kinetic parameters could be ruled out.

Δ*pH-driven Transport*—To investigate ΔpH-driven transport of NhaA, the dependence of the transient currents after a pH jump at different symmetrical Na^+ concentrations was

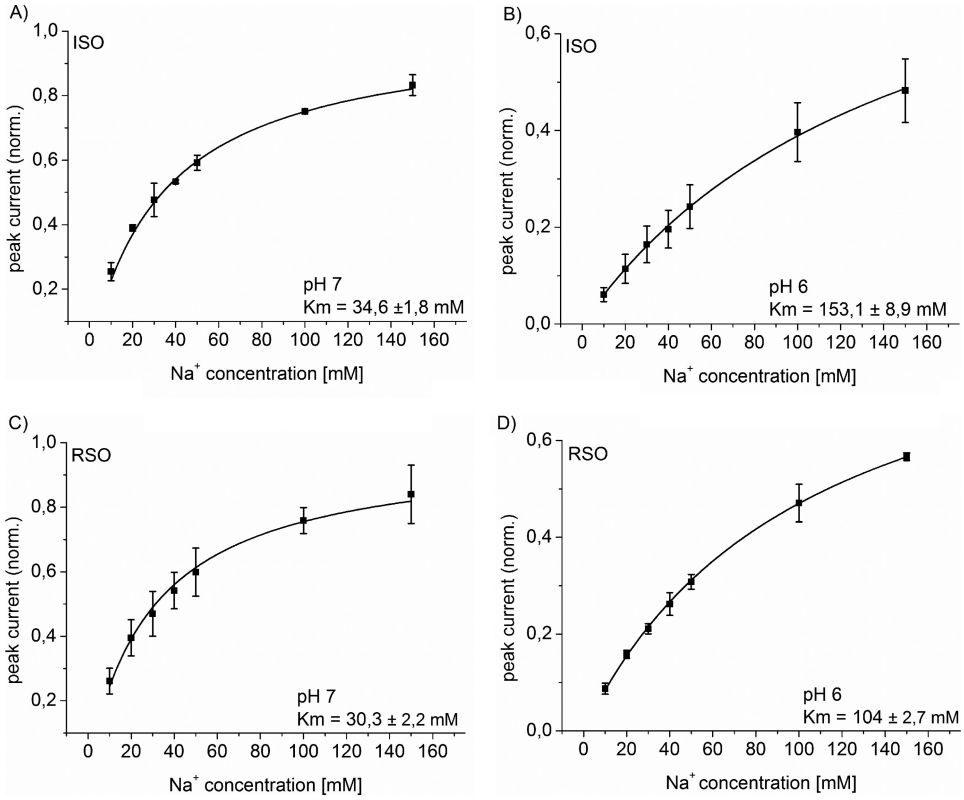

FIGURE 4. **Na^+ concentration dependence of G338S NhaA at optimal and acidic pH.** The transient currents were recorded after a Na^+ concentration jump using the single solution exchange protocol. *A* and *B*, normalized peak currents with ISO membrane vesicles are shown. *C* and *D*, normalized peak currents with RSO proteoliposomes (LPR = 10) are shown. The graphs show average values from recordings using three individual sensors and the corresponding S.D. Normalization was as described under "Experimental Procedures." For the Na^+ concentration jumps, activating solutions containing *x* mM NaCl and (300 – *x*) mM KCl titrated to the indicated pH values with Tris were used. The nonactivating solutions contained 300 mM KCl instead. In addition, all buffers contained 5 mM $MgCl_2$, 25 mM Tris, 25 mM MOPS, 25 mM MES, and 1 mM DTT. The *solid line* is a fit to the data using a hyperbolic model function with a half-saturation concentration K_m and a fixed $v_{max} = 1$.

studied (Fig. 5) using wt NhaA, RSO proteoliposomes. A pH jump from high to low pH corresponds to transport in the forward direction (high pH inside, low pH outside the liposomes), and a pH jump from low to high pH reflects transport in the reverse direction. As a consequence, pH jumps from pH 8.5 to 7, 6, or 5 generated transient currents of positive sign. In contrast, pH jumps from pH 5, 6, or 7 to pH 8.5 resulted in negative currents. As a control, pH jumps in the absence of sodium were recorded. These pH artifact currents are most probably due to an interaction of protons with lipid headgroups (29). They were small (approximately a factor of 10 smaller than at 50 mM Na^+), and their peak currents were subtracted from the corresponding peak currents measured in the presence of Na^+.

For optimal timing of the experimental steps, the equilibration time needed to attain symmetrical Na^+ concentrations after a Na^+ concentration change was determined. First ΔpH-induced currents were measured in the presence of 1.25 mM Na^+. After incubation at a Na^+ concentration of 100 mM for 1 h, much larger ΔpH-induced currents were recorded. Subsequently, a Na^+ concentration of 1.25 mM was reestablished. After an incubation time >6 min, the initial low current amplitude was obtained again. Therefore, after a change in Na^+ concentration, the SSM was incubated for 6 min at the new concentration before the currents were recorded.

Using different pH concentration jump protocols, positive (forward mode) and negative (reverse mode) currents could be generated. These currents were of a comparable magnitude as the ΔNa-driven currents at pH 8.5 (see Fig. 5 A for a comparison). Interestingly the ΔpH-driven currents persisted without a detectable diminishment down to an acidic pH as low as pH 5. Fig. 5, *B* and *C*, shows the pH dependence of the peak currents. For comparison, the currents are normalized to the peak current of the ΔNa signal at pH 8.5 and 100 mM Na^+. The reverse mode currents (Fig. 5 C) were somewhat smaller than the ΔNa signal and independent of pH. The forward mode currents (Fig. 5*B*) were pH-dependent and at pH 5.0 were substantially larger than the ΔNa signal.

We also investigated the Na^+ dependence of the ΔpH-driven currents (Fig. 5, *F–K*). The ΔpH-driven currents in forward transport direction yielded K_m values that seem to be distributed around an average $K_m^{Na} \sim 2.5$ mM, which is significantly lower than the value of ~10 mM obtained in ΔNa-driven transport (Table 1). In the reverse transport direction, K_m^{Na} increased with lower pH inside. The high K_m^{Na} obtained at cytoplasmic pH 6 and 5 (9.5 and 27 mM, Fig. 5, *I* and *K*) may indicate a slight asymmetry of the transporter, which is only apparent at cytoplasmic pH 5–6 and, therefore, was not detected in ΔNa-driven transport at symmetrical pH, where the currents disappear at pH < 6.5. The asymmetry may be related to an acidic-induced conformational change as observed recently by cryomicroscopy (11) and biochemistry (4).

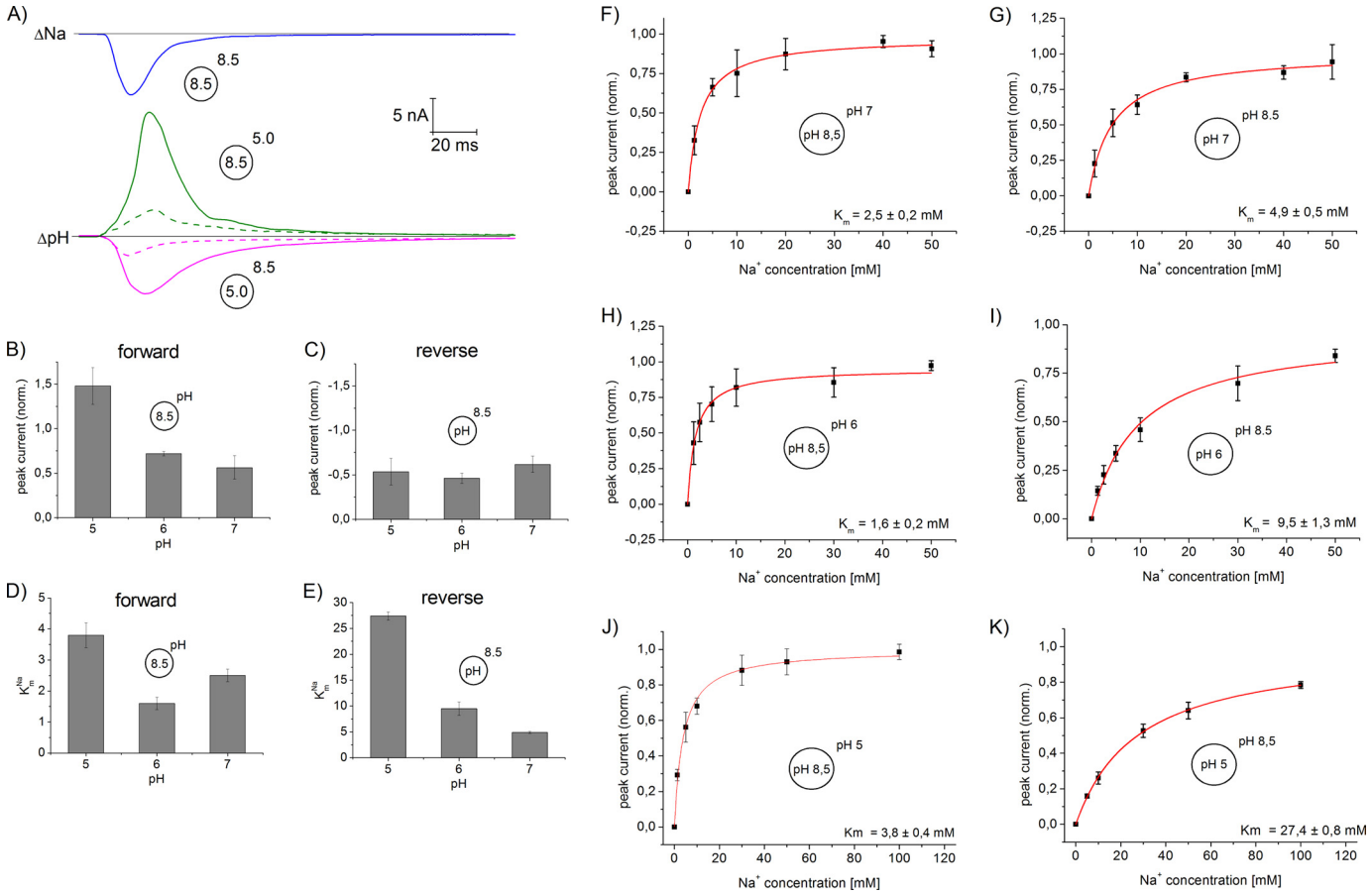

FIGURE 5. **Transient currents after a pH jump using wt NhaA RSO proteoliposomes (LPR = 50).** The currents were measured by means of the single solution exchange protocol. *A*, for comparison, a ΔNa (100 mM) signal was recorded using the same sensor (*upper trace*). The ΔpH signals (*lower traces*) show a solution exchange from pH 8.5 to 5.0 or from pH 5.0 to 8.5 at a symmetrical Na^+ concentration of 100 mM. The *circle* represents the liposome, and the numbers represent the pH inside and outside. For comparison, the corresponding control signal with K^+ instead of Na^+ is given (*dashed lines*). *B*, shown are peak currents at different pH values and a symmetrical Na^+ concentration of 100 mM normalized to the ΔNa peak current shown in *A*. Solution exchange from pH 8.5 to the indicated pH is shown. *C*, shown are peak currents at different pH values and a symmetrical Na^+ concentration of 100 mM normalized to the ΔNa peak current shown in *A*. Solution exchange from the indicated pH to pH 8.5 is shown. *D* and *E*, K_m^{NA} for the measurements shown in panels (*F*, *G*, *H*, *I*, *J*, and *K*). *Panels F*, *G*, *H*, *I*, *J*, and *K* show the normalized peak currents after a pH jump at different symmetrical Na^+ concentrations. Average values from recordings using 3 individual sensors and the corresponding S.D. are displayed. Normalization is as described under "Experimental Procedures." For measurement conditions, the ΔNa signal was recorded using the conditions described in Fig. 2 for 100 mM Na^+ and pH 8.5. For the ΔpH signals, the solutions contained *x* mM NaCl and (300 –*x*) mM KCl. In addition, buffers (*F–I*) contained 5 mM $MgCl_2$, 25 mM Tris, 25 mM MOPS, 25 mM MES, and 1 mM DTT. Buffers (*J* and *K*) additionally contained 5 mM $MgCl_2$, 25 mM Tris, 25 mM MOPS, 25 mM citrate, and 1 mM DTT.

Transport Activity of G338S NhaA at Alkaline pH—Above pH 9.5, an irreversible decrease of the transient currents was observed, limiting our measurements to pH values ≤9.5. To investigate the kinetics of NhaA at a pH above its optimal value, we took advantage of the fact that the optimal pH of G338S NhaA is shifted to acidic pH compared with the wt. Interestingly, at pH 8.5 the transient current of G338S NhaA is biphasic, which is indicative of a presteady-state component in the currents. Because 10 mM Na^+ concentration jumps were used, the contribution of solution exchange artifacts can be neglected.

In Fig. 6 the shape of the transient currents generated by G338S NhaA after a 10 mM Na^+ concentration jump at different pH values was compared. At pH 6.0 the currents show a monophasic decay, although at pH 8.5 the transients became biphasic. In ΔNa-driven transport, biphasic transients were not observed at any other investigated pH value. Biphasic transient currents were also observed in other transporters (30, 31) where the fast transient peak current was identified as a presteady-state charge displacement due to a rapid electrogenic step after substrate binding, whereas the slowly decaying component was shown to represent the steady-state turnover of the transporter. By reconstructing the transporter current (see "Experimental Procedures") we were able to extract the steady-state current from these measurements. For comparison, peak currents and reconstructed steady-state currents are shown in Fig. 2. Using the reconstructed steady-state currents, we could also determine the Na^+ dependence of G338S NhaA at alkaline pH and obtained a value of $K_m^{Na} = 4$ mM.

Essentially the same behavior was found in forward and reverse transport direction. The biphasic transient turned into a much larger monophasic current when the pH inside the RSO proteoliposomes or ISO membrane vesicles was lowered to pH 6.0 while keeping the outside pH at 8.5. This was accomplished by means of a two-step solution exchange protocol as described under "Experimental Procedures." The SSM was first incubated in a Na^+-free resting solution at pH 6.0. Then, a proton gradient of ΔpH = 2.5 was established by exchanging the resting

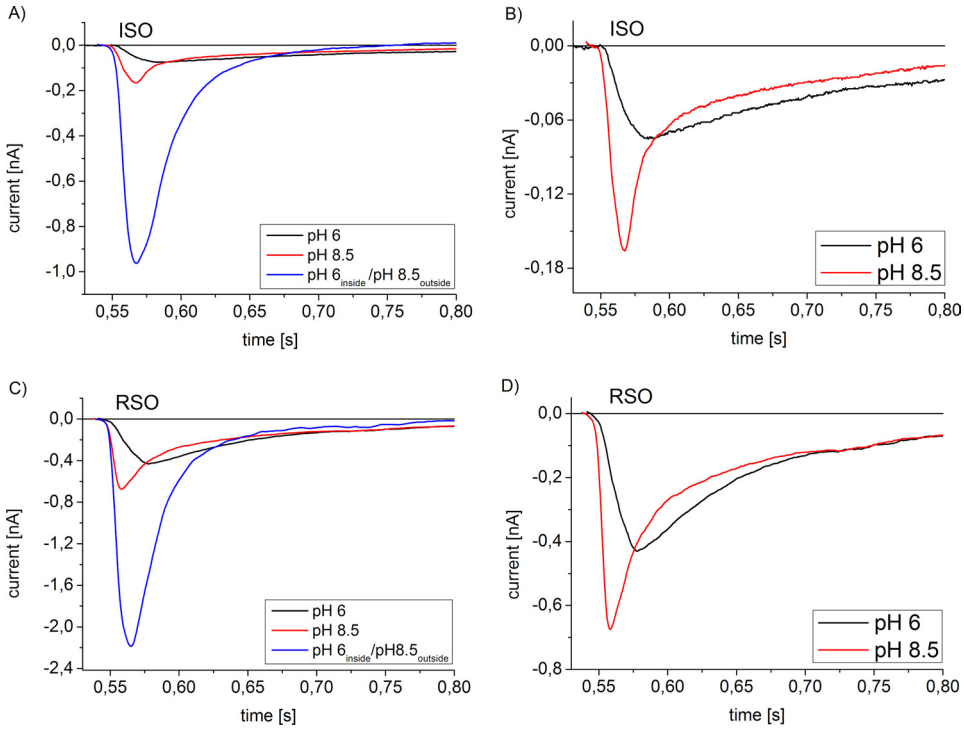

FIGURE 6. **Transient currents of G338S NhaA at alkaline pH.** For comparison, the transient currents after a 10 mM Na^+ concentration jump at a symmetric pH of 6 (*black*) and 8.5 (*red*) were measured with a single solution exchange protocol. For the pH gradient measurements (*blue*), the double solution exchange protocol was used. *A*, G338S ISO membrane vesicles are shown. *C*, G338S RSO proteoliposomes (LPR = 10) are shown. For the Na^+ concentration jumps, activating solutions containing 10 mM NaCl and 290 mM KCl titrated to pH 6 (*black*) or pH 8.5 (*red* and *blue*) with HCl or Tris were used. The nonactivating solutions contained 300 mM KCl titrated to the same pH as the corresponding activating solutions. The resting solutions for the establishment of the ΔpH (*blue*) contained 300 mM KCl at pH 6 (*blue*). In addition, all buffers contained 5 mM $MgCl_2$, 25 mM Tris, 25 mM MOPS, 25 mM MES, and 1 mM DTT. *B* and *D*, shown are the same data as in *A* and *C*. For a better comparison, an expanded view of the transient currents is given.

solution by the nonactivating solution at pH 8.5. Finally, transport was initiated by a 10 mM Na^+ concentration jump via the activating solution with pH 8.5. Therefore, during activation with Na^+, the pH inside the RSO proteoliposomes or ISO membrane vesicles was 6.0 and 8.5 outside, contributing an additional driving force.

Probing Conformational Changes of wt NhaA Using Tryptic Digestion—Proteolysis by trypsin as a means of investigating structural changes of NhaA showed that helix IX at K249 changed conformation with pH (6, 19). To investigate the influence of Na^+ on the conformational change of helix IX, we performed trypsin digestions in the absence of Na^+ as well as in the presence of 10 or 100 mM Na^+ at pH 6.5, 7.5, and pH 8.5 (Fig. 7.). The amount of digested NhaA increased with elevated pH. At pH 6.5 as well as at pH 8.5 no significant influence of Na^+ on trypsin digestion could be monitored. However, at pH 7.5, the amount of digested NhaA increased significantly with the Na^+ concentration.

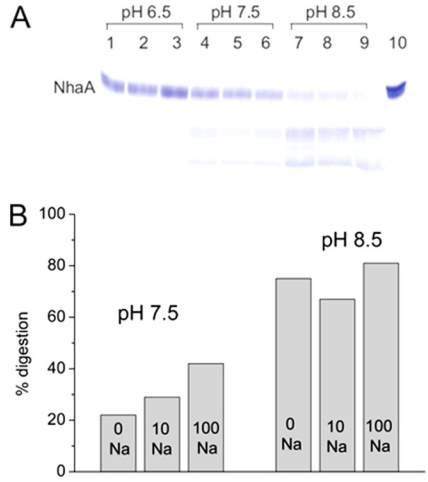

FIGURE 7. **Na^+ and pH dependence of tryptic digestion of wt NhaA.** Trypsin digestion of purified NhaA was conducted in the absence (*lanes 1*, *4*, and *7*) or presence of 10 mM Na^+ (*lanes 2*, *5*, and *8*) and 100 mM Na^+ (*lanes 3*, *6*, and *9*) at the indicated pH values. *A*, the digestion products were resolved on SDS-PAGE with a control of undigested NhaA (*lane 10*). *B*, the extent of digestion was determined by analysis of the density of the gel bands shown in *A*. The experiment was repeated three times with practically identical results.

DISCUSSION

Because of the wealth of structural and functional information available for the *E. coli* NhaA Na^+/H^+ exchanger, this transporter can serve as an example for the mechanistic principles that govern exchanger function in general. In this electrophysiological study we have revealed the mechanism of substrate transport and pH regulation of NhaA using the wt transporter as well as the pH-shifted G338S variant.

The NhaA Antiporter Is Functionally Highly Symmetrical—The use of ISO membrane vesicles and of RSO proteoliposomes enabled us to determine the kinetic parameters of NhaA in the forward and in the reverse transport modes (Fig. 2). Due to the nature of our experimental membrane preparation, a membrane potential was not present in our measurements. This allows a direct comparison of the kinetic parameters of forward and reverse transport without the asymmetry imposed by a membrane potential. At the same time the membrane potential

has to be taken into account if conclusions concerning the physiological role of NhaA are drawn on the basis of the kinetic parameters determined here.

The transport parameters summarized in Table 1 correspond to ΔNa-driven transport at symmetrical pH conditions. The parameters obtained in both directions are surprisingly similar. This supports the concept that only a single substrate binding site is relevant for transport in both directions and argues in favor of a conventional alternating access model.

H^+ and Na^+ Compete for a Common Binding Site—An interesting property of NhaA is the pH dependence of the half-saturation constant for Na^+, K_m^{Na} (see Table 1). A simple explanation of this behavior is coupled Na^+/H^+ binding equilibria (32). In such a kinetic model both substrates Na^+ and H^+ compete for a unique binding site that can either accommodate a Na^+ or one or two H^+ ions. This is similar to the mechanism found in the multidrug transporter EmrE (33, 34).

The pH dependence of NhaA shows a characteristic bell shape, implying that on the acidic as well as on the alkaline side of an optimal pH value the transporter is down-regulated. Qualitatively the same dependence is found for the G338S variant apart from a shift of the optimal pH value to low pH. What is the mechanism of down-regulation at low and high pH?

Down-regulation in the acidic pH range is a K_m effect and is brought about by competition of H^+ and Na^+ for a common binding site. This is reflected by the high K_m^{Na} determined at acidic pH (Table 1). At the same time the maximal activity (V_{max}) of the transporter at saturating Na^+ is only slightly dependent on pH (see "Results") in this pH range, which confirms the proposed competition mechanism.

At the alkaline side of the pH range K_m^{Na} decreases even with increasing pH (K_m^{Na} = 4 mM, see "Results"). Note that the latter could only be measured using the pH-shifted G338S variant, but is assumed to be true also for the wt. The decrease of the transport activity in this pH range must, therefore, be attributed to a decrease of V_{max}, as predicted by the minimal kinetic model discussed below.

ΔpH Versus ΔNa-driven Transport—Under physiological conditions NhaA works as a Na^+ export system driven by the proton motive force to keep the intracellular Na^+ concentration low in a high salt environment. We have, therefore, studied the Na^+ dependence of the NhaA transport activity at symmetrical Na^+ concentration and in the presence of a driving pH gradient (Fig. 5). A remarkable finding is the persistently high transport activity at pH 5 whether low pH is at the cytoplasmic or the periplasmic side of the transporter (Fig. 5, *B* and *C*). This argues against a pH sensor shutting off NhaA at acidic pH. At symmetrical pH conditions, however, transport ceases at pH < 6.5 (Fig. 2) obviously because the H^+ ions effectively compete with Na^+ at the binding site. Hence, under our experimental conditions, pH regulation in NhaA functions exclusively via its active site.

Interestingly, K_m^{Na} can be significantly lower in ΔpH-driven transport (see Fig. 5, *D* and *E*). Values for K_m^{Na} as low as 1.6 mM are obtained in the forward ΔpH-driven mode. This is still higher than the previously determined values of 0.2 mM (10) and 0.1 mM (3). The reason for the discrepancy is unclear.

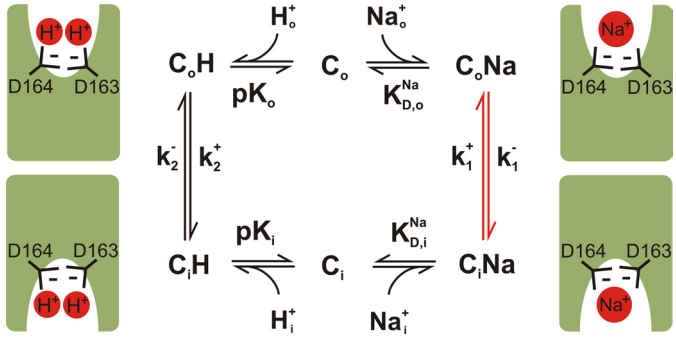

FIGURE 8. **Minimal kinetic model used for the analysis of the transport properties of NhaA.** Outward-facing transporter C_o binds substrates either H^+_o or Na^+_o from the outward (periplasmic) medium, and inward facing carrier C_i binds substrates either H^+_i or Na^+_i from the inward (cytoplasmic) medium. The schematics show the proposed transport mechanism (see "Discussion"). The conformational transitions $C_oH \leftrightharpoons C_iH$ and $C_oNa \leftrightharpoons C_iNa$ are associated with a displacement of the two negatively charged aspartate residues (Asp-163, Asp-164) and one Na^+ or two H^+ ions, respectively. In the case of Na^+ translocation, this leads to a net charge displacement as indicated by *red arrows*. Note that in the crystal structure obtained at pH 4.0 Asp-163 is occluded.

G338S NhaA Is a pH-shifted wt NhaA—The pH dependences of wt and G338S NhaA in Fig. 2 show a striking similarity both in forward and reverse mode, the only difference being a pH shift by ~1.8 pH units. Also the Na^+ dependence of G338S NhaA parallels that of the wild type. The same pH dependence of K_m^{Na} is found for the mutant (Table 1) if the pH shift is taken into account. Therefore, G338S NhaA presents itself as a pH-shifted wt NhaA. This is also apparent in the kinetic model presented below where the mutant can be described by a single p*K* value (as does the wt) shifted by ~1.8 pH units to lower pH. Indeed, Gly-338 is close to the putative "active site" of NhaA (4) and could be envisioned to modulate the pK of the H^+/Na^+ binding site by steric interactions.

G338S NhaA has been previously described as "practically pH-independent at pH 7–9" using an assay where the periplasmic side of the membrane is always at low pH. Down-regulation at alkaline pH does not take place under these conditions, which leads to a flat pH dependence at pH >7 and accounts for the discrepancy with our measurement.

The fact that the functional properties of G338S NhaA can be explained by a simple pK shift compared with the wild type transporter supports the concept that the pH dependence of NhaA is an exclusive property of its active center and, therefore, a consequence of its transport mechanism. If the mutation at position 338 would simply extend the transporter activity to acidic pH by an allosteric pH regulation mechanism, the bell-shaped activity curve would be broadened instead of being just shifted.

A Minimal Kinetic Model Explains the Kinetic Properties of NhaA—To analyze the transport properties of NhaA in more detail we have employed a minimal kinetic model (Fig. 8) that includes only a single common binding site for Na^+ and H^+. Substrate binding and release is assumed to be in rapid equilibrium and is described by dissociation constants for Na^+ (K_D^{Na}) and H^+ (pK_a). The rate-determining reactions are the conformational transitions between the outward facing conformation (C_o) and the inward facing conformation (C_i). A reversible transport model is adopted with forward and

backward rate constants of the conformational transition. Because the experimental data suggest a symmetric transporter, the same kinetic parameters were used for the binding sites in the inward- and outward-facing conformations, and forward and backward rate constants of the two conformational transitions were taken to be the same. This by itself satisfies the law of detailed balance. The kinetic equations describing the model were analytically solved (see the supplemental Fig. 3), and the pH dependence of steady-state turnover was calculated and fitted to the data.

Fig. 9 shows a fit of the minimal kinetic model to the data of Figs. 2, 3, and 4. The pH dependence at two Na^+ concentrations and the Na^+ dependence at two pH values were simultaneously fitted. The K_D^{Na} and pK_a obtained in the fit are given in Fig 9. Because the fit was independent of the absolute values of the rate constants k_1 and k_2, we used the ratio k_1/k_2 as an adjustable fit parameter. In consequence, this model has only five independent fitting parameters; two scaling parameters for the pH dependence and the Na^+ dependence, K_D^{Na}, pK_a, and the ratio k_1/k_2. The low number of parameters ensures that they can be reliably determined by the fit.

In conclusion, a minimal symmetrical kinetic model with a single binding site that is alternatively occupied by Na^+ or H^+ describes well our electrophysiological data set of wt NhaA and the G338S variant and predicts correctly their Na^+ and pH dependence. The Na^+ dissociation constants are similar (3–12 mM), whereas the p*K* for the mutant relative to wt is shifted by ~1.8 pH units into the acidic range. We, therefore, propose that the kinetic principles operative in the model apply also to the transporter. For the forward mode this means that acidic pH prevents effective formation of C_iNa at the cytoplasmic side of the transporter and slows down turnover. Alkaline pH shifts the H^+ binding equilibrium at the periplasmic side of the transporter to the C_o form, thereby slowing down the return of the H^+-loaded carrier to the cytoplasmic side. Note that the minimal model is essentially an ideal alternative access model.

pH Regulation in NhaA—The dramatic pH dependence of NhaA between pH 6.5 to 8.5 was verified using various techniques like $^{22}Na^+$ efflux (3), pH-sensitive dyes (6, 7, 9, 35), and electrophysiology (28). In addition, several conformational-sensitive methods detected conformational transitions at alkaline pH and in a pattern reflecting the pH dependence of NhaA activity (6, 7, 10, 36). Interestingly some of these assays are affected by the presence of Na^+ (36). Na^+/H^+ competition is also apparent in the transporter conformation detected by tryptic digestion (Fig. 7), suggesting involvement of the active site. These results, which have recently been confirmed by cryoelectron microscopy (11), therefore, agree with our results and most probably are related to the transport mechanism. Indeed, this concept can account for the pH dependence observed in previous measurements that were made at either symmetrical pH ($^{22}Na^+$ efflux from NhaA proteoliposomes (3)), or the pH was varied at the Na^+ uptake side of the protein (fluorescence dequenching assay (6, 37). Under these conditions, high H^+ concentration prevents effective Na^+ binding, thereby inhibiting transport. On the other hand, in the ΔpH measurements of Fig. 5, the Na^+ uptake side was always at high pH, allowing for effective Na^+ binding and high turnover.

In other cases the conformational changes leading to activation are suggested to act in a manner distinct from substrate transport. A pH sensor/transducer has been proposed on the basis of mutants that exhibit a pH profile different from that of the wild type. The crystal revealed that these mutations cluster at the N terminus and the N-terminal part of helix IX remote from the active site (13).

Our study presented here shows that below pH 7, NhaA is virtually inactive at symmetrical pH conditions. In contrast, using asymmetrical pH with a high pH at the Na^+ uptake side, a high transport activity was observed in both transport directions down to pH 5 (Fig. 5). In particular, at pH 5.0 at the cytoplasmic side of the transporter, where hypothetically the pH sensor is located, the transporter is highly active. Therefore, the pH-induced conformational transitions proposed to down-regulate the transporter are either irrelevant to the physiological pH response of NhaA or are not observed under our experimental conditions. In that respect it may be of importance that the timescale of the biochemical measurements is ~100 times longer than that of the electrophysiological experiments.

In conclusion, pH regulation by competing Na^+ and H^+ ions at the active site is consistent with our electrophysiological results as well as those of certain previous studies using biochemical methods. However, a few discrepancies still remain as, for instance, the at least 10-fold lower apparent K_m^{NA} using the $^{22}Na^+$ transport assay or the fluorescence quenching assay, the 1000-fold activity increase when raising pH by only 1 unit reported in $^{22}Na^+$ uptake measurements (3), and the effect of mutations remote from the active site on the pH profile (4). Further work is needed to clarify these discrepancies.

A Transport Mechanism for NhaA—A transporter is most effective if it is "asymmetric"; that is, its "affinity" for the pumped substrate is high at the "uptake side" and low at the "release side" (38). In NhaA, the interaction with the asymmetrically distributed counter-substrate creates the asymmetry. The pH dependence of Na^+ transport by NhaA can be described with a single Na^+ binding site with $K_D \sim 3$ mM. By competitive interaction of Na^+ and H^+ at the binding sites, basic pH at the Na^+ uptake side of the transporter creates a low K_m of ~10 mM, whereas at the release side at acidic pH, the K_m ~ 100 mM (Table 1). This enables effective counter-transport of Na^+ and H^+.

An interesting observation is the biphasic nature of the transient currents generated by G338S NhaA at pH 8.5 after a Na^+ concentration jump. This presteady-state current component can only be observed at sufficiently basic pH 8.5, because there turnover is low. The two phases of the transient current represent an electrogenic reaction after Na^+ binding followed by slow steady-state turnover as observed previously for MelB (31). We may conclude from the polarity of the transient current that during the Na^+-induced electrogenic reaction, negative charge is transported to the sodium release side of the protein, and as the G338S mutation does not involve charged residues, this also holds true for the wild type transporter. We, therefore, have to conclude that Na^+ translocation in the NhaA reaction cycle is associated with the displacement of negative charge across the membrane.

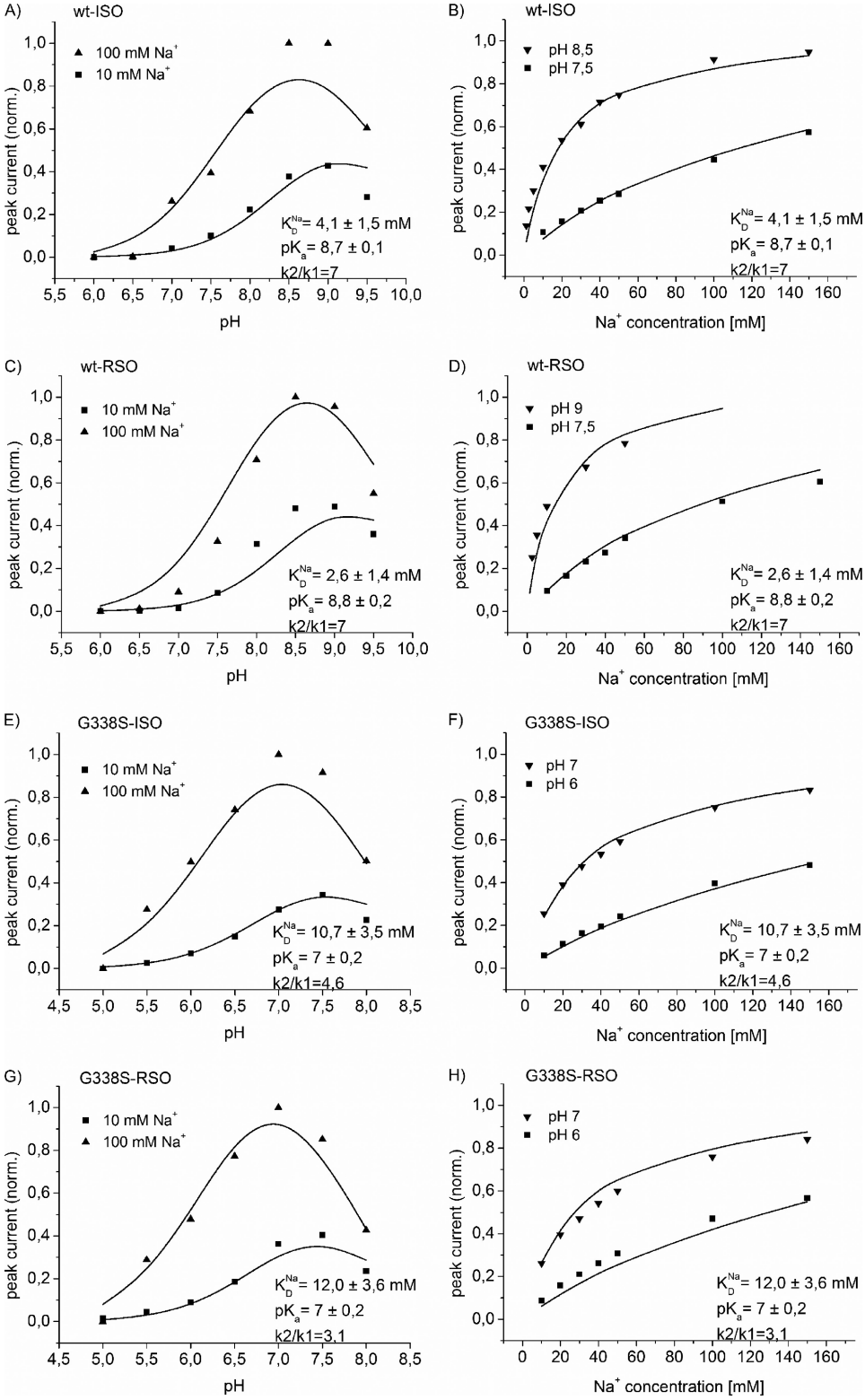

FIGURE 9. **Simultaneous fit of the pH dependence and the sodium dependence of the peak currents to the minimal kinetic model.** The graph shows sodium jump-induced peak currents of wt NhaA and G338S NhaA in native transport direction (*A*, *B*, *E*, and *F*) and reverse transport direction (*C*, *D*, *G*, and *H*). Data and conditions are as in Figs. 2–4. The *solid line* is a fit to the minimal kinetic model described in the "Discussion." The kinetic parameters obtained by the fit are given in the figure.

In fact, negatively charged residues have been proposed to constitute the Na^+ binding site: Asp-163 and Asp-164 (and possibly also Asp-133 (19)). Their charge is only partly compensated by the co-transported Na^+ ion, which suggests a plausible transport mechanism for NhaA (Fig. 8); the conformational transition of the Na^+-loaded carrier ($C_iNa \leftrightharpoons C_oNa$) is associated with the displacement of two negatively charged aspartate residues plus the Na^+ ion, resulting in the

displacement of one net negative charge, in agreement with our measurement. During the conformational transition of the H^+ loaded carrier ($C_oH \leftrightharpoons C_iH$) the two H^+ ions fully compensate the two negative aspartate charges leading to an electroneutral reaction.

The importance of electrogenicity of NhaA for bacterial pH homeostasis has been stressed previously on the basis of thermodynamic arguments (1). But also kinetically electrogenic partial reactions are crucial for proper functioning of the transporter. Using the kinetic model of Fig. 8 and the parameters determined in Fig. 9 ($K_D^{Na} = 2.6$ mM, $pK_a = 8.8$, $k_2/k_1 = 7$), the K_m for Na^+ can be calculated at a given pH. The effect of the potential can be taken into account using potential dependent rate constants k_1 and k_2 (see supplemental Fig. 3) and assuming that Na^+ translocation is electrogenic and H^+ translocation is not. If a single negative charge is displaced during Na^+ translocation, the calculated K_m for Na^+ at pH 8.5 decreases at the cytoplasmic side from 13 to 1.2 mM when a membrane potential of −200 mV is applied. This demonstrates how the strong negative bacterial membrane potential ensures effective Na^+ extrusion even at the low Na^+ concentrations, characteristic for the intracellular medium.

Human Na^+/H^+ antiporters play a primary role in health and disease (39). In contrast to NhaA, the well characterized Na^+/H^+ antiporter NHE1 is electroneutral, its main duty being the excretion of H^+ from cells (26, 40). According to its function, NHE1 is active at acidic, and down-regulated at alkaline cytoplasmic pH. We propose that the mechanistic principles of pH regulation revealed for NhaA are also operative in the eukaryotic antiporter NHE1. Indeed, in the framework of our kinetic model, alkaline down-regulation of NHE1 can be explained by substrate depletion at the Na^+ release side as observed at pH 9.5 in NhaA.

Acknowledgments—We thank Mihaela Cernescu and Guus Erkens for preliminary measurements, Lina Hatahet for excellent technical assistance, and Ernst Bamberg for support of the project.

REFERENCES

1. Padan, E., Bibi, E., Ito, M., and Krulwich, T. A. (2005) *Biochim. Biophys. Acta* **1717,** 67–88
2. Brett, C. L., Donowitz, M., and Rao, R. (2005) *Am. J. Physiol. Cell Physiol.* **288,** 223C–239C
3. Taglicht, D., Padan, E., and Schuldiner, S. (1991) *J. Biol. Chem.* **266,** 11289–11294
4. Padan, E., Kozachkov, L., Herz, K., and Rimon, A. (2009) *J. Exp. Biol.* **212,** 1593–1603
5. Rothman, A., Gerchman, Y., Padan, E., and Schuldiner, S. (1997) *Biochemistry* **36,** 14572–14576
6. Gerchman, Y., Rimon, A., and Padan, E. (1999) *J. Biol. Chem.* **274,** 24617–24624
7. Venturi, M., Rimon, A., Gerchman, Y., Hunte, C., Padan, E., and Michel, H. (2000) *J. Biol. Chem.* **275,** 4734–4742
8. Karasawa., A., Tsuboi, Y., Inoue, H., Kinoshita, R., Nakamura, N., and Kanazawa, H. (2005) *J. Biol. Chem.* **280,** 41900–41911
9. Tzubery, T., Rimon, A., and Padan, E. (2008) *J. Biol. Chem.* **283,** 15975–15987
10. Herz, K., Rimon, A., Olkhova, E., Kozachkov, L., and Padan, E. (2010) *J. Biol. Chem.* **285,** 2211–2220
11. Appel, M., Hizlan, D., Vinothkumar, K. R., Ziegler, C., and Kühlbrandt, W. (2009) *J. Mol. Biol.* **388,** 659–672
12. Dzafić, E., Klein, O., Screpanti, E., Hunte, C., and Mäntele, W. (2009) *Spectrochim. Acta A Mol. Biomol. Spectrosc.* **72,** 102–109
13. Padan, E. (2008) *Trends Biochem. Sci.* **33,** 435–443
14. Galili, L., Herz, K., Dym, O., and Padan, E. (2004) *J. Biol. Chem.* **279,** 23104–23113
15. Galili, L., Rothman, A., Kozachkov, L., Rimon, A., and Padan, E. (2002) *Biochemistry* **41,** 609–617
16. Rimon, A., Gerchman, Y., Kariv, Z., and Padan, E. (1998) *J. Biol. Chem.* **273,** 26470–26476
17. Jardetzky, O. (1966) *Nature* **211,** 969–970
18. Abramson, J., Smirnova, I., Kasho, V., Verner, G., Kaback, H. R., and Iwata, S. (2003) *Science* **301,** 610–615
19. Hunte, C., Screpanti, M., Venturi, M., Rimon, A., Padan, E., and Michel, H. (2005) *Nature* **435,** 1197–1202
20. Arkin, I. T., Xu, H., Jensen, M. Ø., Arbely, E., Bennett, E. R., Bowers, K. J., Chow, E., Dror, R. O., Eastwood, M. P., Flitman-Tene, R., Gregersen, B. A., Klepeis, J. L., Kolossváry, I., Shan, Y., and Shaw, D. E. (2007) *Science* **317,** 799–803
21. Olkhova, E., Hunte, C., Screpanti, E., Padan, E., and Michel, H. (2006) *Proc. Natl. Acad. Sci. U.S.A.* **103,** 2629–2634
22. Olkhova, E., Padan, E., and Michel, H. (2007) *Biophys. J.* **92,** 3784–3791
23. Schulz, P., Garcia-Celma, J. J., and Fendler, K. (2008) *Methods* **46,** 97–103
24. Venturi, M., and Padan, E. (2002) in *A Practical Guide to Membrane Protein Purification* (Hunte, C., Von Jagow, G., and Schagger, H., eds) 2nd Ed., pp. 179–190, Amsterdam
25. Everberg, H., Clough, J., Henderson, P., Jergil, B., Tjerneld, F., and Ramírez, I. B. (2006) *J. Chromatogr. A* **1118,** 244–252
26. Fuster, D., Moe, O. W., and Hilgemann, D. W. (2008) *J. Gen. Physiol.* **132,** 465–480
27. Adler, L. W., Ichikawa, T., Hasan, S. M., Tsuchiya, T., and Rosen, B. P. (1977) *J. Supramol. Struct.* **7,** 15–27
28. Zuber, D., Krause, R., Venturi, M., Padan, E., Bamberg, E., and Fendler, K. (2005) *Biochim. Biophys. Acta* **1709,** 240–250
29. Garcia-Celma, J. J., Hatahet, L., Kunz, W., and Fendler, K. (2007) *Langmuir* **23,** 10074–10080
30. Garcia-Celma, J. J., Ploch, J., Smirnova, I., Kaback, H. R., and Fendler, K. (2010) *Biochemistry* **49,** 6115–6121
31. Meyer-Lipp, K., Séry, N., Ganea, C., Basquin, C., Fendler, K., and Leblanc, G. (2006) *J. Biol. Chem.* **281,** 25882–25892
32. Ganea, C., and Fendler, K. (2009) *Biochim. Biophys. Acta* **1787,** 706–713
33. Yerushalmi, H., and Schuldiner, S. (2000) *Biochemistry* **39,** 14711–14719
34. Yerushalmi, H., and Schuldiner, S. (2000) *FEBS Lett.* **476,** 93–97
35. Kozachkov, L., Herz, K., and Padan, E. (2007) *Biochemistry* **46,** 2419–2430
36. Tzubery, T., Rimon, A., and Padan, E. (2004) *J. Biol. Chem.* **279,** 3265–3272
37. Rosen, B. P. (1986) *Methods Enzymol.* **125,** 328–336
38. Stein, W. D. (1986) *Transport and Diffusion across Cell Membranes*, pp. 404–409, Academic Press, Inc., Orlando. FL
39. Malo, M. E., and Fliegel, L. (2006) *Can. J. Physiol. Pharmacol.* **84,** 1081–1095
40. Aronson, P. S. (1985) *Annu. Rev. Physiol.* **47,** 545–560